

Discrete Flux and Velocity Fields of Probability and Their Global Maps in Reaction Systems

Anna Terebus¹, Chun Liu², and Jie Liang^{1,*},

¹ Department of Bioengineering, University of Illinois at Chicago, Chicago IL, 60607, USA

² Department of Applied Mathematics, Illinois Institute of Technology, Chicago IL, 60616, USA

* Corresponding author, jliang@uic.edu

Abstract

Stochasticity plays important roles in reaction systems. Vector fields of probability flux and velocity characterize time-varying and steady-state properties of these systems, including high probability paths, barriers, checkpoints among different stable regions, as well as mechanisms of dynamic switching among them. However, conventional fluxes on continuous space are ill-defined and are problematic when at boundaries of the state space or when copy numbers are small. By re-defining the derivative and divergence operators based on the discrete nature of reactions, we introduce new formulations of discrete fluxes. Our flux model fully accounts for the discreteness of both the state space and the jump processes of reactions. The reactional discrete flux satisfies the continuity equation and describes the behavior of the system evolving along directions of reactions. The species discrete flux directly describes the dynamic behavior in the state space of the reactants such as the transfer of probability mass. With the relationship between these two fluxes specified, we show how to construct time-evolving and steady-state global flow-maps of probability flux and velocity in the directions of every species at every microstate, and how they are related to the outflow and inflow of probability fluxes when tracing out reaction trajectories. We also describe how to impose proper conditions enabling exact quantification of flux and velocity in the boundary regions, without the difficulty of enforcing artificial reflecting conditions. We illustrate the computation of probability flux and velocity using three model systems, namely, the birth-death process, the bistable Schlögl model, and the oscillating Schnakenberg model.

Keywords: Stochastic biochemical reaction networks, discrete flux and velocity fields of probability

1 INTRODUCTION

Biochemical reactions in cells are intrinsically stochastic [1–4]. When the concentrations of participating molecules are small or the differences in reaction rates are large, stochastic effects become prominent [3, 5–7]. Many stochastic models have been developed to gain understanding of these reaction systems [8–12]. These models either generate time-evolving landscapes of probabilities over different microstates [9–12], or generate trajectories along which the systems travel [8, 13]. Vector fields of probability flux and probability velocity are also of significant interest, as they can further characterize time-varying properties of the reaction systems, including that of the non-equilibrium steady states [14–19]. For example, determining the probability flux can help to infer the mechanism of dynamic switching among different attractors [20, 21]. Quantifying the probability flux can also help to characterize the departure of non-equilibrium reaction systems from detailed balance [16, 22, 23], and can help to identify barriers and checkpoints between different stable cellular states [24]. Computing probability fluxes and velocity fields has found applications in studies of stem cell differentiation [25], cell cycle [24], and cancer development [26, 27].

Models of probability fluxes and velocities in well-mixed mesoscopic chemical reaction systems have been the focus of many studies [17, 18, 20, 22–24, 28–32]. They are often based on the formulation of the Fokker-Planck and the Langevin equations, both involving the assumption of Gaussian noise of two moments [17–19, 23, 24, 33]. However, these models are not valid when copy numbers of molecular species are small [28, 34–36], as they do not provide a full account of the stochasticity of the system [28, 34–38]. For example, the Fokker-Planck model fails to capture multistability in gene regulation networks with slow switching between the ON and the OFF states [36]. These models are also of inadequate accuracy when systems are far from equilibrium [35]. Moreover, solving the systems of partial differential equations resulting from the Fokker-Planck and Langevin Equations requires explicit boundary conditions for states where one or more molecular species have zero copies [18]. These boundary conditions are ill-defined in the context of Gaussian noise [39] and are difficult to impose using the Fokker-Planck/Langevin formulation, or any other continuous models, as reactions cannot occur on boundary states when one or more reactants are exhausted.

Several discrete models of probability flux and velocity based on continuous-time Markov jump processes associated with the firing of reactions have also been introduced [20, 29, 30, 32]. However, these models have limitations. The models developed in [20, 32] account only for outflow fluxes. While the probability of transition to a subsequent microstate after a reaction jump is accounted for, the inflow flux describing the probability of transition into the current microstate from a previous state is not explicitly considered. The work in [40] studies the phosphorylation and dephosphorylation process. It introduces a formulation of discrete flux based on a forward finite difference operator. However, this is only applicable to this special system of simple single-species reactions, where there is no mass exchange between the two different molecular types. The models developed in [29, 30] are limited to analysis of single reactional trajectories. In addition, the probability flux is often assumed to be associated with reactions that are reversible [41]. While these models offer an in-the-moment view on how probability mass moves in the system by following trajectories generated from reaction events, they do not offer a global picture of the time-evolving probability flux at a specific time or at fixed locations in the state space. To construct the global flow-map of discrete probability flux and velocity, proper formulations of discrete flux and velocity, as well as methods to quantify the discrete forward and backward flux between every two states connected by reactions are required.

In this study, we introduce the appropriate formulations of discrete flux and discrete velocity for arbitrary mesoscopic reaction systems. We redefine the derivative operator and discrete divergence based on the discrete nature of chemical reactions. The discreteness of both the state space and the jump processes of reactions is taken into consideration, with the discrete version of the continuity equation satisfied. Our approach allows the quantification of probability flux and velocity at every microstate, as well as the ability in tracing out the outflow probability fluxes and the inflow fluxes as reactions proceeds. In addition, proper boundary conditions are imposed so vector fields of flux and velocity can be exactly computed anywhere in the discrete state space, without the difficulty of enforcing artificial reflecting conditions at the boundaries [42]. Our method can be used to exactly quantify transfer of probability mass and to construct the global flow-map of the probability flux in all allowed directions of reactions over the entire state space. Results computed using our model can provide useful characterization of the dynamic behavior of the reaction system, including the high probability paths along which the probability mass of the system evolves, as well as properties of their non-equilibrium steady states.

The accurate construction of the discrete probability flux, velocity, and their global flow-maps requires the accurate calculation of the time-evolving probability landscape of the reaction networks. Here we employ the recently developed ACME method [12, 43] to compute the exact time-evolving probability landscapes of networks by solving the underlying discrete Chemical Master Equation (dCME). This eliminates potential problems arising from inadequate sampling, where rare events of low probability are difficult to quantify using techniques such as the stochastic simulations algorithm (SSA) [8, 13, 44].

This paper is organized as follows. We first briefly discuss the theoretical framework of reaction networks and discrete Chemical Master Equation. We then introduce the concept of ordering of the microstates of the system, the definitions of discrete derivatives and divergence, as well as flux and velocity on a discrete state space. We further illustrate how time-evolving probability flux and velocity fields can be computed for three classical systems, namely, the birth-death process [12, 45], the bistable Schlögl model [13, 46], and the

oscillating Schnakenberg system [18, 47, 48].

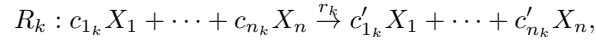
2 Models and Methods

2.1 Microstates, Probability, Reaction and Probability Vector

Microstate and state space. We consider a well-mixed biochemical system with constant volume and temperature. It has n molecular species X_i , $i = 1, \dots, n$, which participate in m reactions R_k , $k = 1, \dots, m$. The *microstate* $\mathbf{x}(t)$ of the system at time t is a column vector of copy numbers of the molecular species: $\mathbf{x}(t) \equiv (x_1(t), x_2(t), \dots, x_n(t))^T \in \mathbb{Z}_+^n$, where all values are non-negative integers. All the microstates that the system can reach form *the state space* $\Omega = \{\mathbf{x}(t) | t \in (0, \infty)\}$. The size of the state space is denoted as $|\Omega|$.

Probability and probability landscapes. The probability of the system to be at a particular microstate \mathbf{x} at time t is denoted as $p(\mathbf{x}, t) \in \mathbb{R}_{[0,1]}$. The probability surface or landscape $\mathbf{p}(t)$ over the state space Ω is denoted as $\mathbf{p}(t) = \{p(\mathbf{x}, t) | \mathbf{x} \in \Omega\}$.

Reaction, discrete increment, and reaction direction. A *reaction* R_k takes the general form of



so that R_k brings the system from a microstate \mathbf{x} to $\mathbf{x} + \mathbf{s}_k$, where the stoichiometry vector

$$\mathbf{s}_k \equiv (s_k^1, \dots, s_k^n) \equiv (c'_{1k} - c_{1k}, \dots, c'_{nk} - c_{nk})$$

gives the unit vector of *the discrete increment* of reaction R_k . \mathbf{s}_k also defines *the direction of the reaction* R_k . In a well-mixed mesoscopic system, the reaction propensity function $A_k(\mathbf{x})$ is determined by the product of the intrinsic reaction rate r_k and the combinations of relevant reactants in the current microstate \mathbf{x} :

$$A_k(\mathbf{x}) = r_k \prod_{l=1}^n \binom{x_l}{c_{lk}}.$$

Discrete Chemical Master Equation and boundary states. The discrete Chemical Master Equation (dCME) is a set of linear ordinary differential equations describing the changes of probability over time at each microstate of the system [8, 49–51]. The dCME for an arbitrary microstate $\mathbf{x} = \mathbf{x}(t)$ can be written in the general form as:

$$\frac{\partial p(\mathbf{x}, t)}{\partial t} = \sum_{k=1}^m [A_k(\mathbf{x} - \mathbf{s}_k) p(\mathbf{x} - \mathbf{s}_k, t) - A_k(\mathbf{x}) p(\mathbf{x}, t)], \quad \mathbf{x} - \mathbf{s}_k, \mathbf{x} \in \Omega. \quad (1)$$

It is possible that only a subset or none of the permissible reactions can occur at a particular state \mathbf{x} if it is at the boundary of the state space Ω , where the number of reactants is inadequate. Specifically, we define *the boundary states* $\partial\Omega_k$ for reaction k as the states where reaction R_k cannot happen:

$$\partial\Omega_k \equiv \{\mathbf{x} = (x_1, \dots, x_i, \dots, x_n) \mid \text{there exist } i : x_i < c_{ik}\}. \quad (2)$$

We define the overall boundary states as $\partial\Omega \equiv \bigcup_{k=1}^m \partial\Omega_k$.

Reactional probability vector and its time-derivative. We can consider each of the k -th reactions separately and decompose the right hand side of Eq. (1) into m components, one for each reaction, $k = 1 \dots m$:

$$\frac{\partial p_k(\mathbf{x}, t)}{\partial t} = A_k(\mathbf{x} - \mathbf{s}_k) p(\mathbf{x} - \mathbf{s}_k, t) - A_k(\mathbf{x}) p(\mathbf{x}, t). \quad (3)$$

$\partial p(\mathbf{x}, t) / \partial t$ in Eq.(1) therefore can also be written as:

$$\frac{\partial p(\mathbf{x}, t)}{\partial t} = \sum_{k=1}^m \frac{\partial p_k(\mathbf{x}, t)}{\partial t}.$$

Any of the m reactions can alter the value of $p(\mathbf{x}, t)$ as specified by Eq.(3). While the probability $p(\mathbf{x}, t)$ is a scalar, we define *the reactional probability vector* $\mathbf{p}(\mathbf{x}, t)$ such that

$$\mathbf{p}(\mathbf{x}, t) = (p_1(\mathbf{x}, t), \dots, p_m(\mathbf{x}, t)) \in \mathbb{R}^m, \quad (4)$$

with $p(\mathbf{x}, t) = \mathbf{p}(\mathbf{x}, t) \cdot \mathbf{1} = (p_1(\mathbf{x}, t), \dots, p_m(\mathbf{x}, t)) \cdot (1, \dots, 1)^T = \sum_{k=1}^m p_k(\mathbf{x}, t)$. We also define the *time-derivative of the probability vector* $\partial \mathbf{p}(\mathbf{x}, t) / \partial t$ as:

$$\frac{\partial \mathbf{p}(\mathbf{x}, t)}{\partial t} \equiv \left(\frac{\partial p_1(\mathbf{x}, t)}{\partial t}, \dots, \frac{\partial p_m(\mathbf{x}, t)}{\partial t} \right),$$

and we have:

$$\frac{\partial p(\mathbf{x}, t)}{\partial t} = \left(\frac{\partial p_1(\mathbf{x}, t)}{\partial t}, \dots, \frac{\partial p_m(\mathbf{x}, t)}{\partial t} \right) \cdot (1, \dots, 1)^T = \frac{\partial \mathbf{p}(\mathbf{x}, t)}{\partial t} \cdot \mathbf{1} = \sum_{k=1}^m \frac{\partial p_k(\mathbf{x}, t)}{\partial t}.$$

2.2 Ordering Microstates, Directional Derivative, and Discrete Divergence

Ordering Microstates. As the microstates are discrete and the stochastic jumps are dictated by the discrete increments $\{\mathbf{s}_k\}$ of reactions, we introduce *discrete partial derivative* and *discrete divergence* to describe effect of specific reactions.

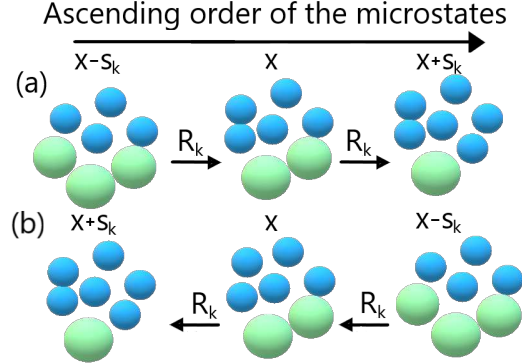


Figure 1: Ordering of microstates: a) when the order of the state preceding the reaction R_k and the state after the reaction coincides with the imposed ascending order of microstates, we have $\mathbf{x} - \mathbf{s}_k \prec \mathbf{x} \prec \mathbf{x} + \mathbf{s}_k$; b) when the order of the state preceding the reaction R_k and the state after the reaction is in the opposite direction to the ascending order of the microstates, we have $\mathbf{x} + \mathbf{s}_k \prec \mathbf{x} \prec \mathbf{x} - \mathbf{s}_k$.

First, we imposed an unambiguous order relationship " \prec " over all microstates. We impose an ascending order on the microstates $\mathbf{x}^0 \prec \mathbf{x}^1 \prec \dots \prec \mathbf{x}^{|\Omega|}$ that is maintained at all time, such that for each pair of states $\mathbf{x}^i \neq \mathbf{x}^j$, either $\mathbf{x}^i \prec \mathbf{x}^j$ or $\mathbf{x}^j \prec \mathbf{x}^i$ holds, but not both. There are many ways to impose such an ordering. Without loss of generality, we can first use the lexicographic order so the microstates are initially sorted by species alphabetically, and then by increasing number of molecules of the species. Other ordering schemes are also possible.

Discrete Partial Derivative. We now consider reactional component $p_k(\mathbf{x}, t)$ of the probability of the state \mathbf{x} (see Eq.(4)). For reaction R_k , the only possible change in \mathbf{x} is determined by its discrete increment of \mathbf{s}_k .

We first consider the case when the state $\mathbf{x} - \mathbf{s}_k$ preceding the reaction R_k and the state \mathbf{x} after the reaction have the order $\mathbf{x} - \mathbf{s}_k \prec \mathbf{x}$. This also implies $\mathbf{x} \prec \mathbf{x} + \mathbf{s}_k$. In this case, the direction of the reaction

coincides with the direction of the imposed ordering of the microstates (Figure 1a). We define the *discrete partial derivative* $\Delta p_k(\mathbf{x}, t)/\Delta \mathbf{x}_k$ of $p_k(\mathbf{x}, t)$ over the discrete states in the direction \mathbf{s}_k of reaction R_k as:

$$\frac{\Delta p_k(\mathbf{x}, t)}{\Delta \mathbf{x}_k} \equiv p_k(\mathbf{x}, t) - p_k(\mathbf{x} - \mathbf{s}_k, t), \quad (5)$$

if $\mathbf{x} - \mathbf{s}_k \prec \mathbf{x} \prec \mathbf{x} + \mathbf{s}_k$.

We now consider the case when $\mathbf{x} \prec \mathbf{x} - \mathbf{s}_k$, namely, when the state $\mathbf{x} - \mathbf{s}_k$ preceding reaction R_k and the state \mathbf{x} after R_k are ordered such that the after-reaction state \mathbf{x} is placed prior to the before-reaction state $\mathbf{x} - \mathbf{s}_k$. This also implies $\mathbf{x} + \mathbf{s}_k \prec \mathbf{x}$ (Figure 1b). In this case, the discrete partial derivative $\Delta p_k(\mathbf{x}, t)/\Delta \mathbf{x}_k$ is defined as:

$$\frac{\Delta p_k(\mathbf{x}, t)}{\Delta \mathbf{x}_k} \equiv -(p_k(\mathbf{x}, t) - p_k(\mathbf{x} + \mathbf{s}_k, t)), \quad (6)$$

if $\mathbf{x} + \mathbf{s}_k \prec \mathbf{x} \prec \mathbf{x} - \mathbf{s}_k$. The negative sign “-” indicates that the direction of the reaction R_k is opposite to the direction of the imposed order of the states.

Discrete Divergence. We now introduce the *discrete divergence* $\nabla_d \cdot \mathbf{p}(\mathbf{x}, t) \in \mathbb{R}$ for the probability vector $\mathbf{p}(\mathbf{x}, t)$ over the m discrete increments $\{\mathbf{s}_k\}$ of the reactions. Applying Eq.(5)–(6) to each reactional component $p_i(\mathbf{x}, t)$ of $\mathbf{p}(\mathbf{x}, t)$ defined in Eq.(4), the discrete divergence $\nabla_d \cdot \mathbf{p}(\mathbf{x}, t)$ at \mathbf{x} is the sum of all discrete partial derivatives along the directions of reactions:

$$\nabla_d \cdot \mathbf{p}(\mathbf{x}, t) \equiv \sum_{k=1}^m \frac{\Delta p_k(\mathbf{x}, t)}{\Delta \mathbf{x}_k}. \quad (7)$$

2.3 Discrete Flux and Velocity at a Fixed Microstate

Single-Reactional Flux. There are two types of reaction events affecting flux between two states \mathbf{x} and $\mathbf{x} + \mathbf{s}_k$: reactions generating flux flowing from \mathbf{x} to $\mathbf{x} + \mathbf{s}_k$, and reactions generating flux flowing from $\mathbf{x} + \mathbf{s}_k$ to \mathbf{x} . The ordering of the microstates enables unique definition of the type of events that the firing of a reaction R_k belongs to. For any two states \mathbf{x} and $\mathbf{x} + \mathbf{s}_k$, only one of the two orderings is possible: we have either $\mathbf{x} \prec \mathbf{x} + \mathbf{s}_k$, or $\mathbf{x} + \mathbf{s}_k \prec \mathbf{x}$. We define the *single-reactional flux of probability* $J_k(\mathbf{x}, t) \in \mathbb{R}$ for reaction R_k at microstate $\mathbf{x} \in \Omega$ as:

$$J_k(\mathbf{x}, t) \equiv \begin{cases} A_k(\mathbf{x})p(\mathbf{x}, t), & \mathbf{x} \prec \mathbf{x} + \mathbf{s}_k, \\ A_k(\mathbf{x} - \mathbf{s}_k)p(\mathbf{x} - \mathbf{s}_k, t), & \mathbf{x} \prec \mathbf{x} - \mathbf{s}_k. \end{cases} \quad (8)$$

$J_k(\mathbf{x}, t)$ depicts the change in $p(\mathbf{x}, t)$ at the state \mathbf{x} due to one firing of reaction R_k . If $\mathbf{x} \prec \mathbf{x} + \mathbf{s}_k$, $J_k(\mathbf{x}, t)$ depicts the outward flux (outflux) of probability due to one firing of reaction R_k at \mathbf{x} to bring the system from \mathbf{x} to $\mathbf{x} + \mathbf{s}_k$. If $\mathbf{x} \prec \mathbf{x} - \mathbf{s}_k$, $J_k(\mathbf{x}, t)$ depicts the inward flux (influx) of probability due to one firing of reaction R_k at $\mathbf{x} - \mathbf{s}_k$ to bring the system from $\mathbf{x} - \mathbf{s}_k$ to \mathbf{x} . For any two states connected by a reaction R_k , only one of two orderings is possible as the imposed ordering of the states is unique. Therefore, the single-reactional flux can be applied to all microstates in a self-consistent manner. It also accounts for all reactions, as $J_k(\mathbf{x}, t)$ can be defined for every reaction R_k . The *single-reactional R_k velocity* is defined correspondingly as:

$$v_k(\mathbf{x}, t) \equiv J_k(\mathbf{x}, t)/p(\mathbf{x}, t).$$

Flux at Boundary States. No reactions are possible if any of the reactant molecules is unavailable, or if its copy number is inadequate. If $\mathbf{x} \prec \mathbf{x} + \mathbf{s}_k$ (Figure 1a), but $\mathbf{x} \in \partial\Omega_k$ (Eq.(2)), reaction R_k cannot happen, and we have $J_k(\mathbf{x}, t) = 0$. If $\mathbf{x} \prec \mathbf{x} - \mathbf{s}_k$ (Figure 1b), but $\mathbf{x} - \mathbf{s}_k \in \partial\Omega_k$ (Eq.(2)), reaction R_k cannot happen, and we have $J_k(\mathbf{x}, t) = 0$. We therefore have the following boundary conditions for $J_k(\mathbf{x}, t)$:

$$J_k(\mathbf{x}, t) \equiv \begin{cases} 0, & \mathbf{x} \prec \mathbf{x} + \mathbf{s}_k \text{ and } \mathbf{x} \in \partial\Omega_k \\ 0, & \mathbf{x} \prec \mathbf{x} - \mathbf{s}_k \text{ and } \mathbf{x} - \mathbf{s}_k \in \partial\Omega_k \end{cases}$$

Discrete Derivative of J_k . Similar to Eq. (5-6), the directional derivative of single-reactional flux $\Delta J_k(\mathbf{x}, t)/\Delta \mathbf{x}_k$ of $J_k(\mathbf{x}, t)$ along the direction \mathbf{s}_k of reaction R_k is defined as follows:

$$\frac{\Delta J_k(\mathbf{x}, t)}{\Delta \mathbf{x}_k} \equiv \begin{cases} A_k(\mathbf{x})p(\mathbf{x}, t) - A_k(\mathbf{x} - \mathbf{s}_k)p(\mathbf{x} - \mathbf{s}_k, t), & \text{if } \mathbf{x} - \mathbf{s}_k \prec \mathbf{x}, \\ -(A_k(\mathbf{x} - \mathbf{s}_k)p(\mathbf{x} - \mathbf{s}_k, t) - A_k(\mathbf{x} - \mathbf{s}_k + \mathbf{s}_k)p(\mathbf{x} - \mathbf{s}_k + \mathbf{s}_k, t)), & \text{if } \mathbf{x} \prec \mathbf{x} - \mathbf{s}_k. \end{cases}$$

With simplifications from the trivial identity $\underline{-\mathbf{s}_k + \mathbf{s}_k} = 0$, the two expressions of $\Delta J_k(\mathbf{x}, t)/\Delta \mathbf{x}_k$ can be combined into one:

$$\frac{\Delta J_k(\mathbf{x}, t)}{\Delta \mathbf{x}_k} \equiv A_k(\mathbf{x})p(\mathbf{x}, t) - A_k(\mathbf{x} - \mathbf{s}_k)p(\mathbf{x} - \mathbf{s}_k, t) = -\frac{\partial p_k(\mathbf{x}, t)}{\partial t}. \quad (9)$$

Total Reactional Flux, Divergence and Continuity Equation. We now define the *total reactional flux* or *r-flux* $\mathbf{J}_r(\mathbf{x}, t)$, which describes the probability flux at a microstate \mathbf{x} at time t :

$$\mathbf{J}_r(\mathbf{x}, t) \equiv (J_1(\mathbf{x}, t), \dots, J_m(\mathbf{x}, t)) \in \mathbb{R}^m. \quad (10)$$

Intuitively, the r-flux $\mathbf{J}_r(\mathbf{x}, t)$ is the vector of rate change of the probability mass at \mathbf{x} in directions of all reactions. Similar to Eq. (7), we have the *discrete divergence* of $\mathbf{J}_r(\mathbf{x})$ at microstate \mathbf{x} :

$$\nabla_d \cdot \mathbf{J}_r(\mathbf{x}, t) \equiv \sum_{k=1}^m \frac{\Delta J_k(\mathbf{x}, t)}{\Delta \mathbf{x}_k} \quad (11)$$

From Eq. (9) we have:

$$\nabla_d \cdot \mathbf{J}_r(\mathbf{x}, t) = \sum_{k=1}^m [A_k(\mathbf{x})p(\mathbf{x}, t) - A_k(\mathbf{x} - \mathbf{s}_k)p(\mathbf{x} - \mathbf{s}_k, t)]. \quad (12)$$

Similar to its continuous version [31, 52] the discrete continuity equation for the probability mass insists that:

$$\nabla_d \cdot \mathbf{J}_r(\mathbf{x}, t) = -\frac{\partial p(\mathbf{x}, t)}{\partial t}. \quad (13)$$

From Eqs. (11), (13) and (1), it is clear that r-flux $\mathbf{J}_r(\mathbf{x}, t)$ satisfies the continuity equation. The probability mass flows simultaneously along all m directions, with the continuity equation satisfied at all time.

Single-Reactional Species Flux and Stoichiometric Projection. The reactional probability flux $J_k(\mathbf{x}, t)$ along the direction of reaction R_k defined in Eq. (8) can be further decomposed into components of individual species. With the predetermined stoichiometry $\mathbf{s}_k = (s_k^1, \dots, s_k^n)$, we define the *stoichiometric projection* of $J_k(\mathbf{x}, t)$ into the component of the j -th species X_j as:

$$J_k^j(\mathbf{x}, t) \equiv s_k^j J_k(\mathbf{x}, t).$$

The set of scalar components of all species $\{J_k^j(\mathbf{x}, t)\}$ can be used to form a vector $\mathbf{J}_k(\mathbf{x}, t) \in \mathbb{R}^n$, which we call *the single-reaction species flux*:

$$\mathbf{J}_k(\mathbf{x}, t) \equiv (J_k^1(\mathbf{x}, t), \dots, J_k^n(\mathbf{x}, t)) = \mathbf{s}_k J_k(\mathbf{x}, t) \in \mathbb{R}^n.$$

The single-reaction species velocity of probability is defined correspondingly as $\mathbf{v}_k(\mathbf{x}, t) \equiv \mathbf{J}_k(\mathbf{x}, t)/p(\mathbf{x}, t)$.

Total Species Flux and Velocity. The *total species flux* or *s-flux* $\mathbf{J}_s(\mathbf{x}, t) \in \mathbb{R}^n$ is the sum of all k single-reaction species flux vectors at a microstate $\mathbf{x} \in \mathbb{R}^n$:

$$\mathbf{J}_s(\mathbf{x}, t) \equiv \sum_{k=1}^m \mathbf{J}_k(\mathbf{x}, t) = \sum_{k=1}^m \mathbf{s}_k J_k(\mathbf{x}, t) \in \mathbb{R}^n. \quad (14)$$

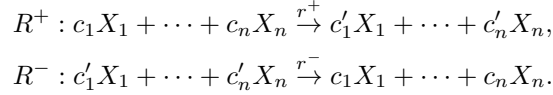
The *total species velocity* for probability is defined accordingly as:

$$\mathbf{v}_s(\mathbf{x}, t) = \sum_{k=1}^m \mathbf{J}_s(\mathbf{x}, t)/p(\mathbf{x}, t). \quad (15)$$

The s-flux $\mathbf{J}_s(\mathbf{x}, t)$ is different from the r-flux $\mathbf{J}_r(\mathbf{x}, t)$ defined in Eq. (12). Reaction-centric $\mathbf{J}_r(\mathbf{x}, t) \in \mathbb{R}^m$ characterizes the total probability flux at current state in the directions of all reactions, while species-centric $\mathbf{J}_s(\mathbf{x}, t) \in \mathbb{R}^n$ sums up the contributions of every reaction to the probability flux at state \mathbf{x} in the directions of all species.

2.4 Flux of reversible reaction

Flux of reversible reactions system. We now discuss probability flux in reversible reaction systems that has been previously studied [16, 53], and how they are related to fluxes formulated here. For a pair of the reactions, its directionality needs to be specified upfront, namely, which reaction is the forward reaction R^+ , and which is the reversed reaction R^- :



Let $\mathbf{s} = (c'_1 - c_1, \dots, c'_n - c_n)$ be the stoichiometry of reaction R^+ , $-\mathbf{s}$ the stoichiometry of reaction R^- . The flux J described in [16, 53] is the net flux between \mathbf{x} and $\mathbf{x} + \mathbf{s}$. It is specified as the difference between the forward flux at \mathbf{x} $J^+(\mathbf{x}, t) = r^+ \prod_{l=1}^n \binom{x_l}{c_l} p(\mathbf{x}, t)$ generated by the forward reaction R^+ and the reverse flux at $\mathbf{x} + \mathbf{s}$ $J^-(\mathbf{x} + \mathbf{s}, t) = r^- \prod_{l=1}^n \binom{x_l + s_l}{c'_l} p(\mathbf{x} + \mathbf{s}, t)$ generated by the reverse reaction R^- , both connecting \mathbf{x} and $\mathbf{x} + \mathbf{s}$ [16, 53]:

$$J(\mathbf{x}, t) = r^+ \prod_{l=1}^n \binom{x_l}{c_l} p(\mathbf{x}, t) - r^- \prod_{l=1}^n \binom{x_l + s_l}{c'_l} p(\mathbf{x} + \mathbf{s}, t). \quad (16)$$

Conversion between single-reactional species flux and flux in a pair of reversible reaction system. The flux $J(\mathbf{x}, t)$ for a pair of reversible reactions above can be related to the s-flux $\mathbf{J}_s(\mathbf{x}, t)$ of Eq. (14) by examining the projection of the $J(\mathbf{x}, t)$ in Eq. (16) to individual species. Specifically, with the stoichiometry \mathbf{s} , the projection of the flux of Eq. (16) to the component of the j -th species X_j is:

$$\mathbf{J}(\mathbf{x}, t) = \mathbf{s}J(\mathbf{x}, t) = \mathbf{s}r^+ \prod_{l=1}^n \binom{x_l}{c_l} p(\mathbf{x}, t) - \mathbf{s}r^- \prod_{l=1}^n \binom{x_l + s_l}{c'_l} p(\mathbf{x} + \mathbf{s}, t) \in \mathbb{R}^n. \quad (17)$$

When the direction of the forward reaction R^+ coincides with the ascending order of the states, one firing of R^+ with the stoichiometry vector \mathbf{s} at the state \mathbf{x} brings the system to the state $\mathbf{x} + \mathbf{s}$ in the direction of the ascending order. From Eq. (14), the s-flux $\mathbf{J}_s(\mathbf{x}, t)$ for (R^+, R^-) is $\mathbf{J}_s(\mathbf{x}, t) = \mathbf{s}r^+ \prod_{l=1}^n \binom{x_l}{c_l} p(\mathbf{x}, t) - \mathbf{s}r^- \prod_{l=1}^n \binom{x_l + s_l}{c'_l} p(\mathbf{x} + \mathbf{s}, t)$. In this case, the projection of the reversible reaction flux by Eq. (17) is identical to the s-flux by Eq. (14) at the state \mathbf{x} .

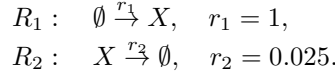
When the direction of the forward reaction R^+ is opposite to the ascending order of the states, one firing of R^- with the stoichiometry vector $-\mathbf{s}$ at the state $\mathbf{x} + \mathbf{s}$ brings the system to the state \mathbf{x} in the direction of the ascending order. From Eq. (14), the s-flux $\mathbf{J}_s(\mathbf{x} + \mathbf{s}, t)$ for (R^+, R^-) is $\mathbf{J}_s(\mathbf{x} + \mathbf{s}, t) = \mathbf{s}r^+ \prod_{l=1}^n \binom{x_l}{c_l} p(\mathbf{x}, t) - \mathbf{s}r^- \prod_{l=1}^n \binom{x_l + s_l}{c'_l} p(\mathbf{x} + \mathbf{s}, t)$. In this case, the projection of the reversible reaction flux by Eq. (17) is identical to s-flux by Eq. (14) at the state $\mathbf{x} + \mathbf{s}$.

3 Results

Below we illustrate how time-evolving and steady-state flux and velocity fields of the probability mass can be computed for three model systems, namely, the birth-death process, the bistable Schlögl model, and the oscillating Schnakenberg system. The underlying discrete Chemical Master Equation (dCME) (Eq.(1)) of these models are solved using the recently developed ACME method [12,43]. The resulting exact probability landscapes of these models are used to compute the flux and the velocity fields.

3.1 The Birth and Death Process

The birth-death process is a simple, but ubiquitous process of the synthesis and degradation of molecule of a single specie [12,45]. The reaction schemes and rate constants examined in this study are specified as follows:



Below we use k as the index of the two reactions.

Ordering Microstates. The microstate in this system is defined by the copy number x of the molecular specie X . We order the microstates in the direction of increasing copy numbers of x , namely, $(x = 0) \prec (x = 1) \prec (x = 2) \dots$.

Discrete Increment and Reaction Direction. Reaction R_1 brings the system from the state x to the state $x + 1$, in the direction of increasing order of the microstates. Its discrete increment is $s_1 = 1$. Reaction R_2 brings the system from the state x to the state $x - 1$, in the direction of decreasing order of the microstates. Its discrete increment is therefore $s_2 = -1$.

Discrete Chemical Master Equation. Following Eq.(1), the discrete Chemical Master Equation for this system can be written as:

$$\partial p(x, t) / \partial t = r_1 p(x, t) - r_1 p(x - 1, t) - r_2(x + 1) \times p(x + 1, t) + r_2 x p(x, t). \quad (18)$$

Single-Reactional Flux, Velocity and Boundary Conditions. The single-reactional flux $J_k(x, t) \in \mathbb{R}$ can be written as:

$$J_1(x, t) = r_1 p(x, t), \quad J_2(x, t) = r_2(x + 1) p(x + 1, t). \quad (19)$$

Here $x = 0, 1, \dots$. No special boundary conditions are required for this system, as $J_1(x, t)$ and $J_2(x, t)$ at the boundary $x = 0$ take the values specified by Eq. (19). The single-reactional velocity $v_k(x, t) \in \mathbb{R}$ can be written as: $v_1(x, t) = J_1(x, t) / p(x, t)$ and $v_2(x, t) = J_2(x, t) / p(x, t)$.

Discrete Partial Derivative. The imposed ordering of the microstates implies $x \prec x + s_1$, as $s_1 = 1$ and $x \prec x + 1$. By Eq. (5), the derivative $\Delta J_1(x, t) / \Delta x_1$ of the single-reactional flux function J_1 is:

$$\frac{\Delta J_1(x, t)}{\Delta x_1} = J_1(x, t) - J_1(x - s_1, t) = r_1 p(x, t) - r_1 p(x - 1, t).$$

The imposed ordering of the microstates also has $x \prec x - s_2$, as $s_2 = -1$ and $x \prec x + 1$. By Eq. (6), the derivative $\Delta J_2(x, t) / \Delta x_2$ of the single-reactional flux function J_2 is:

$$\frac{\Delta J_2(x, t)}{\Delta x_2} = -(J_2(x, t) - J_2(x + s_2, t)) = -(r_2(x + 1) p(x + 1, t) - r_2(x) p(x, t)).$$

Total Reactional Flux, Discrete Divergence, and Continuity Equation. Following Eq. (10), the total reactional flux $\mathbf{J}_r(x, t) \in \mathbb{R}^2$ is:

$$\mathbf{J}_r(x, t) = (J_1(x, t), J_2(x, t)) = (r_1 p(x, t), r_2(x + 1) p(x + 1, t)).$$

The total reactional velocity $\mathbf{v}_r(x, t) \in \mathbb{R}^2$ is: $\mathbf{v}_r(x, t) = \mathbf{J}_r(x, t) / p(x, t)$.

Following Eq. (7), the discrete divergence $\nabla_d \cdot \mathbf{J}_r(x, t)$ of $\mathbf{J}_r(x, t) \in \mathbb{R}^2$ over the discrete increments s_1 and s_2 can be written as:

$$\nabla_d \cdot \mathbf{J}_r(x, t) \equiv \sum_{k=1}^2 \frac{\Delta J_k(x, t)}{\Delta x_k} = r_1 p(x, t) - r_1 p(x-1, t) - r_2(x+1)p(x+1, t) + r_2(x)p(x, t). \quad (20)$$

Here the r-flux $J_r(x, t)$ indeed satisfies the continuity equation, as we have $\nabla_d \cdot \mathbf{J}_r(x, t) = -\partial p(x, t)/\partial t$ from Eqs. (13), (18), and (20).

Stoichiometry projection and single-reactional species flux. Since there is only one specie in this system, the stoichiometry projection of $J_k(x, t)$ to the specie X equals to the single-reactional species flux $\mathbf{J}_k(x, t) \in \mathbb{R}$, which can be written as:

$$\mathbf{J}_1(x, t) = r_1 p(x, t) \quad \text{and} \quad \mathbf{J}_2(x, t) = -r_2(x+1)p(x+1, t).$$

The single-reactional species velocity $\mathbf{v}_k(x, t) \in \mathbb{R}$ can be written as follows: $\mathbf{v}_1(x, t) = J_1(x, t)/p(x, t)$ and $\mathbf{v}_2(x, t) = J_2(x, t)/p(x, t)$.

Total Species Flux and Velocity. Following Eqs. (14)–(15), the s-flux $J_s(x, t)$ and the total velocity $v_s(x, t)$ are:

$$J_s(x, t) = r_1 p(x, t) - r_2(x+1)p(x+1, t),$$

$$v_s(x, t) = J_s(x, t)/p(x, t).$$

When $J_s(x, t) > 0$ and $v_s(x, t) > 0$, the probability mass moves in the direction of increasing copy number of X . This is the direction of the ascending order of microstates we imposed. When $J_s(x, t) < 0$ and $v_s(x, t) < 0$, the probability mass moves in the direction of the decreasing copy number of X . We will further use just simple flux instead of s-flux.

Overall Behavior of the Birth and Death System. We examine the behavior of the birth and death process under the initial conditions $p(x=0)|_{t=0} = 1$ (Figure 2a, backside) and that of the uniform distribution (Figure 2d, backside).

For the initial condition of $p(x=0)|_{t=0} = 1$, the probability landscape changes from that with a peak at $x=0$ to that with a peak at $x=40$ (Figure 2a). Figure 2b shows the heatmap of the flux $J_s(x, t)$, and Figure 2c the heatmap of the velocity $v_s(x, t)$. Yellow and red areas represent locations where the probability moves in the positive direction, while white areas represents locations where the flux and velocity both are close to be zero. The flux and velocity of probability mass (Figure 2b– 2c) are positive at all time, indicating that the probability mass is moving only in the direction of increasing copy number of x . Moreover, when the probability is non-zero, the probability velocity remains constant at any fixed time t across different microstates. The blue line in Figure 2b– 2c corresponds to the peak of the system, that changes its location from $x=0$ to $x=40$.

For the initial condition of the uniform distribution, the probability landscape changes from the constant line to that with a peak at $x=40$ (Figure 2d). Figure 2e shows the heatmap of the flux $J_s(x, t)$, and Figure 2f the heatmap of the velocity $v_s(x, t)$. Blue areas represent locations where the probability mass moves in the negative direction, yellow and red areas represent locations where the probability moves in the positive direction, while white areas represents locations where the flux and velocity both are equal to zero. Specifically, when $x < 40$, we have $J_s(x, t) > 0$ and $v_s(x, t) > 0$, namely, the probability mass moves in the direction of increasing copy number of x . In contrast, when $x > 40$, we have $J_s(x, t) < 0$ and $v_s(x, t) < 0$, indicating that the probability mass moves in the direction of decreasing copy number of x . When $x=40$, we have $J_s(x, t) = 0$ and $v_s(x, t) = 0$. Furthermore, the probability velocity at a specific time t is different for different microstates, with the highest velocities located at the boundary of $x=0$. The blue line in Figure 2e– 2f $x=40$ corresponds to the peak of the system, which appears starting at about $t=5$.

To solve this problem using the ACME method, we introduced the buffer of capacity $x=92$. At the state $x=92$ when the buffer is exhausted, no synthesis reaction can occur. Therefore, the flux at the boundary $x=92$ is set to zero.

Our birth and death system eventually reaches to a steady state. As expected, the same steady state probability distribution is reached from both initial conditions (shown in different scale in Figure 2a and 2d). At the steady state, the probability landscape has a peak at $x = 40$. Both the velocity $v_s(x, t)$ and the flux $J_s(x, t)$ converge to zero at steady state.

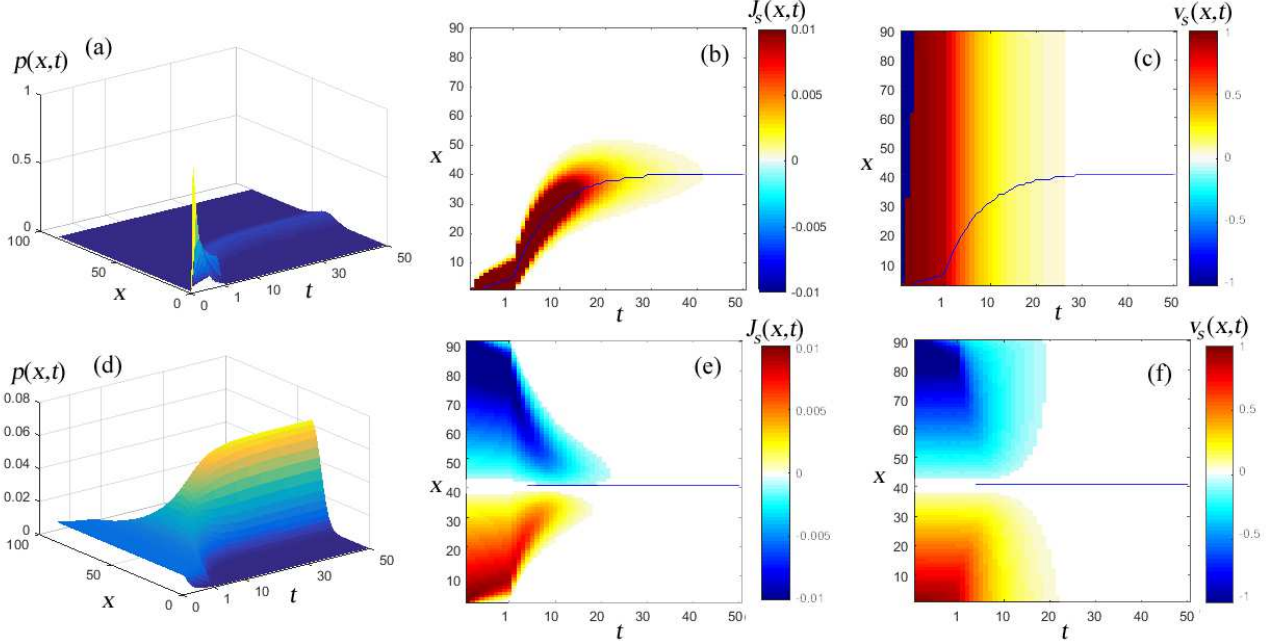
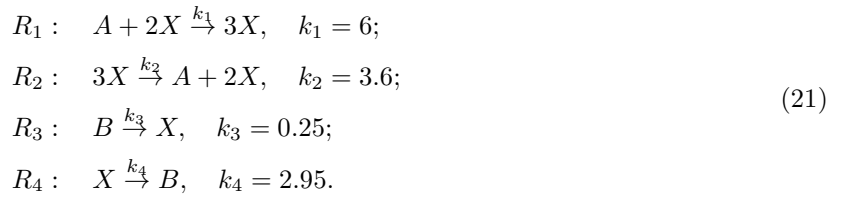


Figure 2: The time-evolving probability landscape, flux and velocity of the probability mass of the birth and death system starting from the initial conditions of $p(x = 0)|_{t=0} = 1$ (a–c) and from the initial conditions of the uniform distribution (d–f). a) and d): the probability landscape in $p(x, t)$; b) and e): the corresponding value of flux $J_s(x, t)$; c) and f): the value of velocity $v_s(x, t)$.

3.2 Bistable Schlögl model

The Schlögl model is a one-dimensional bistable system consisting of an auto-catalytic network involving one molecular specie X and four reactions [46]. It is a canonical model for studying bistability and state-switching [13,54]. The reaction schemes and kinetic constants examined in this study are specified as follows:



Here A and B have constant concentrations a and b , which are set to $a = 1$ and $b = 2$, respectively. We set the volume of the system to $V = 25$ [46]. The rate of reactions are specified as $r_1 = k_1/V$, $r_2 = k_2/V^2$, $r_3 = k_3V$, $r_4 = k_4$.

Ordering Microstates. We define the microstates of this system using the copy number x of the molecular specie X . We order the microstates in the direction of increasing copy numbers of X , namely, $(x = 0) \prec (x = 1) \prec (x = 2) \dots$.

Discrete Increment and Reaction Direction. Reactions R_1 and R_3 bring the system from the state x to the state $x + 1$, in the direction of increasing order of the microstates. Their discrete increments s_1 and s_3 are $s_1 = 1$ and $s_3 = 1$. Reactions R_2 and R_4 bring the system from the state x to the state $x - 1$, in the direction of decreasing order of the microstates. Their discrete increments s_2 and s_4 are therefore $s_2 = -1$ and $s_4 = -1$.

Discrete Chemical Master Equation. Following Eq.(1), the discrete Chemical Master Equation for this system can be written as:

$$\begin{aligned} \frac{\partial p(x, t)}{\partial t} = & r_1 a \frac{(x-1)(x-2)}{2} p(x-1, t) + r_2 \frac{(x+1)x(x-1)}{6} p(x+1, t) + r_3 b p(x-1, t) + r_4 (x+1) \\ & \times p(x+1, t) - r_1 a \frac{x(x-1)}{2} p(x, t) - r_2 \frac{x(x-1)(x-2)}{6} p(x, t) - r_3 b p(x, t) - r_4 x p(x, t). \end{aligned} \quad (22)$$

We compute the probability landscape $p(x, t)$ underlying Eq.(22) using the ACME method [12, 43].

Single-Reactional Flux, Velocity and Boundary Conditions. Following Eq. (8), the single-reactional flux $J_k(x, t) \in \mathbb{R}$ can be written as:

$$\begin{aligned} J_1(x, t) &= r_1 a \frac{x(x-1)}{2} p(x, t), J_2(x, t) = r_2 \frac{(x+1)x(x-1)}{6} p(x+1, t), \\ J_3(x, t) &= r_3 b p(x, t), J_4(x, t) = r_4 (x+1) p(x+1, t). \end{aligned}$$

We have the single-reactional fluxes $J_1(x, t) = 0$ and $J_2(x, t) = 0$ on the boundary with either $x = 0$ or $x = 1$, where reactions R_1 and R_2 cannot happen. The single-reactional fluxes $J_3(x, t)$ and $J_4(x, t)$ are as given above and do not vanish at the boundaries.

The single-reactional velocity $v_k \in \mathbb{R}$ can be written as: $v_k(x, t) = J_k(x, t)/p(x, t)$, with $k = 1, \dots, 4$.

Discrete Partial Derivative. The imposed ordering of the microstates has $x \prec x + 1$, therefore, $x \prec x + s_1$, $x \prec x - s_2$, $x \prec x + s_3$, and $x \prec x - s_4$, as $s_1 = 1$, $s_2 = -1$, $s_3 = 1$, and $s_4 = -1$. According to Eqs. (5) – (6), the derivatives $\Delta J_k(x, t)/\Delta x_k$ of the single-reactional fluxes $\{J_k\}$ are:

$$\begin{aligned} \frac{\Delta J_1(x, t)}{\Delta x_1} &= J_1(x, t) - J_1(x - s_1, t) = r_1 a \frac{x(x-1)}{2} p(x, t) - r_1 a \frac{(x-1)(x-2)}{2} p(x-1, t), \\ \frac{\Delta J_2(x, t)}{\Delta x_2} &= -(J_2(x, t) - J_2(x + s_2, t)) = -(r_2 \frac{(x+1)x(x-1)}{6} p(x+1, t) - r_2 \frac{(x+2)(x+1)x}{6} p(x, t)), \\ \frac{\Delta J_3(x, t)}{\Delta x_3} &= J_3(x, t) - J_3(x - s_3, t) = -(r_3 b p(x, t) - r_3 b p(x-1, t)), \\ \frac{\Delta J_4(x, t)}{\Delta x_4} &= -(J_4(x, t) - J_4(x + s_4, t)) = -(r_4 (x+1) p(x+1, t) - r_4 x p(x, t)). \end{aligned}$$

Total Reactional Flux and Velocity, Discrete Divergence, and Continuity Equation. Following Eq. (10), the total reactional flux $\mathbf{J}_r(x, t) \in \mathbb{R}^4$ is:

$$\begin{aligned} \mathbf{J}_r(x, t) &= (J_1(x, t), J_2(x, t), J_3(x, t), J_4(x, t)) \\ &= (r_1 a \frac{x(x-1)}{2} p(x, t), r_2 \frac{(x+1)x(x-1)}{6} p(x+1, t), r_3 b p(x, t), r_4 (x+1) p(x+1, t)). \end{aligned}$$

The total reactional velocity $\mathbf{v}_r(x, t) \in \mathbb{R}^4$ is: $\mathbf{v}_r(x, t) = \mathbf{J}_r(x, t)/p(x, t)$.

The discrete divergence $\nabla_d \cdot \mathbf{J}_r(x, t)$ of $\mathbf{J}_r(x, t) \in \mathbb{R}^4$ over the discrete increments s_1, s_2, s_3 , and s_4 can be written as:

$$\begin{aligned} \nabla_d \cdot \mathbf{J}_r(x, t) &= \sum_{k=1}^4 \frac{\Delta J_k(x, t)}{\Delta x_k} = -\frac{(x-1)(x-2)}{2} r_1 a p(x-1, t) \\ &+ r_1 a \frac{x(x-1)}{2} p(x, t) - r_2 \frac{(x+1)x(x-1)}{6} p(x+1, t) \\ &+ r_2 \frac{x(x-1)(x-2)}{6} p(x, t) - r_3 b p(x-1, t) + r_3 b p(x, t) \\ &- r_4 (x+1) p(x+1, t) + r_4 x p(x, t). \end{aligned} \quad (23)$$

The flux $\mathbf{J}_R(x, t)$ indeed satisfies the continuity equation, as we have: $\nabla_d \cdot \mathbf{J}_r(x, t) = -\partial p(x, t)/\partial t$ from Eqs. (13), (22), and (23).

Stoichiometry projection and single-reactional species flux. Since there is only one specie x in this system, the stoichiometry projection of single-reactional flux $J_k(x, t)$ to x equals to the single-reactional species flux $\mathbf{J}_k(x, t) \in \mathbb{R}$, which can be written as:

$$\begin{aligned}\mathbf{J}_1(x, t) &= r_1 a \frac{x(x-1)}{2} p(x, t), \\ \mathbf{J}_2(x, t) &= -r_2 \frac{(x+1)x(x-1)}{6} p(x+1, t), \\ \mathbf{J}_3(x, t) &= r_3 b p(x, t), \\ \mathbf{J}_4(x, t) &= -r_4 (x+1) p(x+1, t).\end{aligned}$$

The single-reactional species velocities $\mathbf{v}_k \in \mathbb{R}$ is $\mathbf{v}_k(x, t) = \mathbf{J}_k(x, t)/p(x, t)$, with $k = 1, \dots, 4$.

Total Species Flux and Velocity. Following Eqs. (14)–(15), the total species flux $\mathbf{J}_s(x, t)$ and velocity $\mathbf{v}_s(x, t)$ for the four reactions are :

$$J_s(x, t) = r_1 a \frac{x(x-1)}{2} p(x, t) - r_2 \frac{(x+1)x(x-1)}{6} p(x+1, t) + r_3 b p(x, t) - r_4 (x+1) p(x+1, t),$$

and $v_s(x, t) = J_s(x, t)/p(x, t)$.

Overall Behavior of the Schlögl System. For the set of parameter values used in Eqs. (21), Schlögl model is bistable. It has two peaks at $x = 4$ and $x = 92$. In order to study how switching between the two peaks occur, we examine the behavior of the model under the initial conditions of $p(x = 4)|_{t=0} = 1$ (Figure 3a) and the initial condition of $p(x = 92)|_{t=0} = 1$ (Figure 3d).

For the initial distribution of $p(x = 4)|_{t=0} = 1$, the probability landscape changes from that with a single peak at $x = 4$ to that with two maximum peaks at $x = 4$ and $x = 92$ (Figure 3a). Figure 3b shows the heatmap of the flux $J_s(x, t)$, and Figure 3c the heatmap of the velocity $v_s(x, t)$. Yellow and red areas represent locations where the probability moves in the positive direction, while white areas represents locations where the flux and velocity both are close to be zero. The lower blue lines in Figure 3b– 3c correspond to the peak at $x = 4$. They are straight lines as the location of the peak does not change over time. Another blue line starts to appear at $x = 92$ at about $t = 3$ and corresponds to the second peak. At the same time, at around $t = 3$, we observe the appearance of a minimum of the probability landscape (red line), separating the two maximum peaks. We have $J_s(x, t) > 0$ and $v_s(x, t) > 0$, indicating that the probability moves in the direction of increasing copy number of molecules (Figure 3b– 3c) in the majority of the states. In the white region, we have $J_s(x, t) = 0$ and $v_s(x, t) = 0$.

For the first initial condition of $p(x = 92)|_{t=0} = 1$, the probability landscape changes from that with a single peak at $x = 92$ to that of two peaks at $x = 92$ and $x = 4$ (Figure 3d). Figure 3e shows the heatmap of the flux $J_s(x, t)$, and Figure 3f the heatmap of the velocity $v_s(x, t)$. Blue areas represent locations where the probability mass moves in the negative direction, while white areas represents locations where the flux and velocity both are equal to zero. The top blue lines in Figure 3e– 3f correspond to the peak at $x = 92$. These are straight lines as the location of this peak does not change over time. Another blue line starting to appear at $x = 4$ at around $t = 3$ and corresponds to the second peak. At around $t = 3$, we also observe the appearance of a minimum on the probability landscape (red line) separating the two maximum peaks. In the blue region, we have $J_s(x, t) < 0$ and $v_s(x, t) < 0$, and the probability moves in the direction of increasing copy number of molecules (Figure 3e– 3f) in the majority of states. In the white region, we have $J_s(x, t) = 0$ and $v_s(x, t) = 0$.

In both cases (Figure 3), the second peak appears after about $t = 3$. We also observe that the absolute values of the flux driving the system from the system with one peak at $x = 4$ to the emergence of the second peak at $x = 92$, and from the system with one peak at $x = 92$ to the emergence of the second peak at $x = 4$ are of the same scale.

The Schlögl process eventually reaches to a steady state. As expected, the same steady state probability distribution is reached from both initial conditions. At the steady state, the probability landscape has two

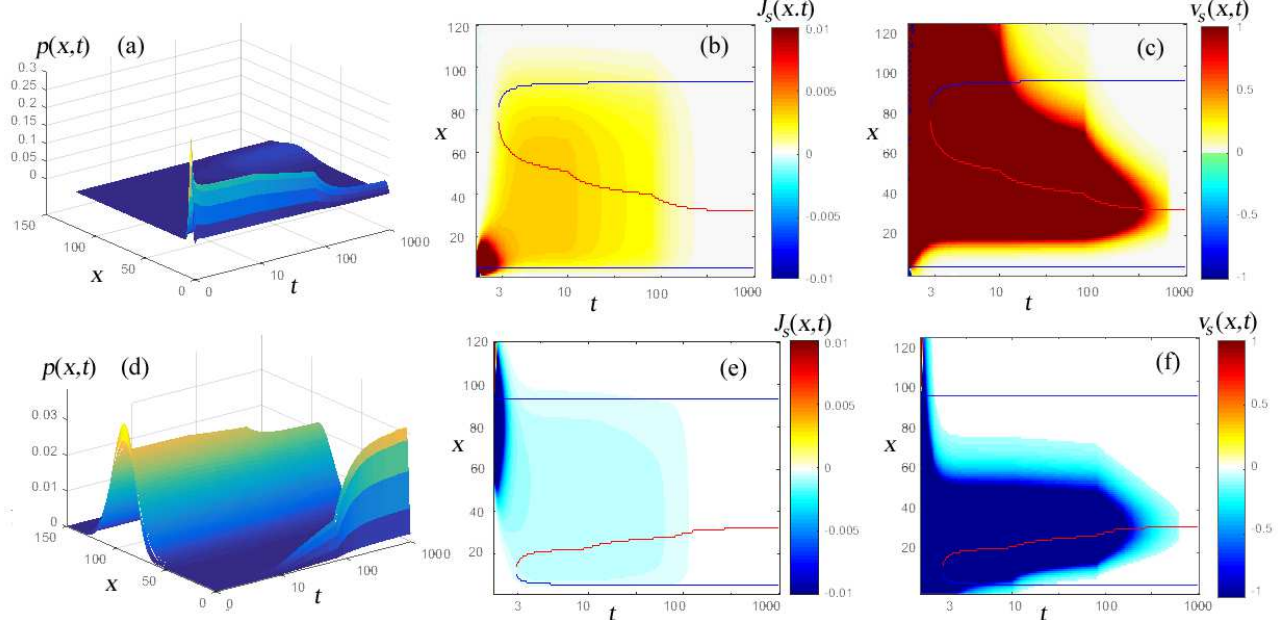
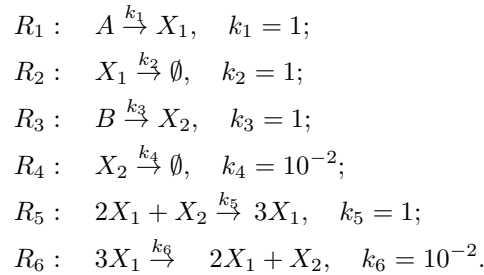


Figure 3: The time-evolving probability landscape, flux and velocity of the probability mass in the Schlögl system starting from the initial conditions of $p(x=4)|_{t=0} = 1$ (a-c) and from the initial conditions of $p(x=92)|_{t=0} = 1$ (d-f). a) and d): the probability landscape in $p(x,t)$; b) and e): the corresponding value of flux in $J_s(x,t)$; c) and f): the value of velocity $v_s(x,t)$.

peaks at $x = 4$ and $x = 92$. Both the velocity $v_s(x,t)$ and the flux $J_s(x,t)$ converge to zero at the steady state.

3.3 Schnakenberg Model

The Schnakenberg model is a simple chemical reaction system originally constructed to study the behavior of limit cycle [55]. It provides an important model for analyzing oscillating behavior in reaction systems [18, 47, 48]. The reaction scheme and rate constants examined in this study are specified as follows:



Here X_1 and X_2 are molecular species whose copy numbers x_1 and x_2 oscillate, A and B are reactants of fixed copy numbers of a and b , respectively. The volume of the system V is set to $V = 10^{-2}$ [55]. The rate of reactions are specified as $r_1 = k_1$, $r_2 = k_2$, $r_3 = k_3$, $r_4 = k_4$, $r_5 = k_5/V^2$, $r_6 = k_6/V^2$.

Ordering Microstates. The microstate $\mathbf{x} = (x_1, x_2)$ in this system is defined by the ordered pair of copy numbers x_1 and x_2 of the molecular species X_1 and X_2 . We impose the ascending order of the microstates first in the direction of the increasing copies of X_1 . At fixed value of X_1 , we then sort the states in the order of increasing copy number of X_2 . We therefore have $(x_1 = 0, x_2 = 0) \prec (x_1 = 0, x_2 = 1) \prec (x_1 = 0, x_2 = 2) \prec \dots \prec (x_1 = 1, x_2 = 0) \prec (x_1 = 1, x_2 = 1) \prec \dots$.

Table 1: Schnakenberg system reactions stoichiometry

Reactions	R_1	R_3	R_5	R_2	R_4	R_6
Discrete Increments	$\mathbf{s}_1 = (1, 0)$	$\mathbf{s}_3 = (0, 1)$	$\mathbf{s}_5 = (1, -1)$	$\mathbf{s}_2 = (-1, 0)$	$\mathbf{s}_4 = (0, -1)$	$\mathbf{s}_6 = (-1, 1)$

Discrete Increment and Reaction Direction. The discrete increments \mathbf{s}_1 , \mathbf{s}_3 , and \mathbf{s}_5 of reactions R_1 , R_3 , and R_5 that bring the system in the direction of increasing order of the microstates and the discrete increments \mathbf{s}_2 , \mathbf{s}_4 , and \mathbf{s}_6 of reactions R_2 , R_4 , and R_6 that bring the system in the direction of the decreasing order of the microstates are listed in Table 1.

Discrete Chemical Master Equation. Following Eq.(1), the discrete Chemical Master Equation for the system can be written as:

$$\begin{aligned}
 \frac{\partial p(\mathbf{x}, t)}{\partial t} = & -r_1 a p(x_1, x_2, t) + r_1 a p(x_1 - 1, x_2, t) - r_2 x_1 p(x_1, x_2, t) + r_2 (x_1 + 1) p(x_1 + 1, x_2, t) \\
 & - r_3 b p(x_1, x_2, t) + r_3 b p(x_1, x_2 - 1, t) + r_4 (x_2 + 1) p(x_1, x_2 + 1, t) - r_4 x_2 p(x_1, x_2, t) \\
 & + r_5 \frac{(x_1 - 1)(x_1 - 2)x_2}{2} p(x_1 - 1, x_2 + 1, t) - r_5 \frac{x_1(x_1 - 1)x_2}{2} p(x_1, x_2, t) \\
 & + r_6 \frac{(x_1 - 1)x_1(x_1 + 1)}{6} p(x_1 + 1, x_2 - 1, t) - r_6 \frac{x_1(x_1 - 1)(x_1 - 2)}{6} p(x_1, x_2, t).
 \end{aligned} \tag{24}$$

We compute the probability landscape $p(\mathbf{x}, t)$ underlying Eq.(22) using the ACME method [12, 43].

Single-Reactional Flux, Velocity and Boundary Conditions. The single-reactional flux $J_k(\mathbf{x}, t) \in \mathbb{R}$ can be written as:

$$\begin{aligned}
 J_1(\mathbf{x}, t) &= r_1 a p(x_1, x_2, t), \\
 J_2(\mathbf{x}, t) &= r_2 (x_1 + 1) p(x_1 + 1, x_2, t), \\
 J_3(\mathbf{x}, t) &= r_3 b p(x_1, x_2, t), \\
 J_4(\mathbf{x}, t) &= r_4 (x_2 + 1) p(x_1, x_2 + 1, t), \\
 J_5(\mathbf{x}, t) &= r_5 \frac{(x_1 - 1)(x_1 - 2)x_2}{2} \\
 &\quad \times p(x_1 - 1, x_2 + 1, t), \\
 J_6(\mathbf{x}, t) &= r_6 \frac{(x_1 - 1)x_1(x_1 + 1)}{6} \\
 &\quad \times p(x_1 + 1, x_2 - 1, t).
 \end{aligned} \tag{25}$$

We have the single-reactional fluxes $J_5(\mathbf{x}, t) = 0$ and $J_6(\mathbf{x}, t) = 0$ on the boundary with either $\mathbf{x} = (0, 0)$ or $\mathbf{x} = (1, 0)$, where reactions R_5 and R_6 cannot happen. The other single-reactional fluxes are as given above and do not vanish at the boundaries.

The single-reactional velocity $v_k(\mathbf{x}, t) \in \mathbb{R}$ can be written as: $v_k(\mathbf{x}, t) = J_k(\mathbf{x}, t)/p(\mathbf{x}, t)$.

Discrete Partial Derivative. The imposed ordering of the microstates has $\mathbf{x} \prec \mathbf{x} + \mathbf{s}_1$, $\mathbf{x} \prec \mathbf{x} - \mathbf{s}_2$, $\mathbf{x} \prec \mathbf{x} + \mathbf{s}_3$, $\mathbf{x} \prec \mathbf{x} - \mathbf{s}_4$, $\mathbf{x} \prec \mathbf{x} + \mathbf{s}_5$, and $\mathbf{x} \prec \mathbf{x} - \mathbf{s}_6$. According to Eqs. (5)– (6), the derivatives

Table 2: Schnakenberg system reactional flux stoichiometry projections

Reaction	$J_k^1(x_1, x_2, t) = s_k^1 J_k(x_1, x_2, t)$	$J_k^2(x_1, x_2, t) = s_k^2 J_k(x_1, x_2, t)$
R_1	$r_1 a p(x_1, x_2, t)$	0
R_2	$-r_2 (x_1 + 1) p(x_1 + 1, x_2, t)$	0
R_3	0	$r_3 b p(x_1, x_2, t)$
R_4	0	$-r_4 (x_2 + 1) p(x_1, x_2 + 1, t)$
R_5	$r_5 \frac{(x_1 - 1)(x_1 - 2)x_2}{2} p(x_1 - 1, x_2 + 1, t)$	$-r_5 \frac{(x_1 - 1)(x_1 - 2)x_2}{2} p(x_1 - 1, x_2 + 1, t)$
R_6	$-r_6 \frac{(x_1 - 1)x_1(x_1 + 1)(x_1 - 2)}{6} p(x_1 + 1, x_2 - 1, t)$	$r_6 \frac{(x_1 - 1)x_1(x_1 + 1)(x_1 - 2)}{6} p(x_1 + 1, x_2 - 1, t)$

$\Delta J_k(\mathbf{x}, t)/\Delta \mathbf{x}_k$ of the single-reactional fluxes J_k can be written as:

$$\begin{aligned}
 \frac{\Delta J_1(\mathbf{x}, t)}{\Delta \mathbf{x}_1} &= J_1(\mathbf{x}, t) - J_1(\mathbf{x} - \mathbf{s}_1, t) = r_1 a p(x_1, x_2, t) - r_1 a p(x_1 - 1, x_2, t), \\
 \frac{\Delta J_2(\mathbf{x}, t)}{\Delta \mathbf{x}_2} &= -(J_2(\mathbf{x}, t) - J_2(\mathbf{x} + \mathbf{s}_2, t)) = -(r_2 (x_1 + 1) p(x_1 + 1, x_2, t) - r_2 x_1 p(x_1, x_2, t)), \\
 \frac{\Delta J_3(\mathbf{x}, t)}{\Delta \mathbf{x}_3} &= J_3(\mathbf{x}, t) - J_3(\mathbf{x} - \mathbf{s}_3, t) = r_3 b p(x_1, x_2, t) - r_3 b p(x_1, x_2 - 1, t), \\
 \frac{\Delta J_4(\mathbf{x}, t)}{\Delta \mathbf{x}_4} &= -(J_4(\mathbf{x}, t) - J_4(\mathbf{x} + \mathbf{s}_4, t)) = -(r_4 (x_2 + 1) p(x_1, x_2 + 1, t) - r_4 x_2 p(x_1, x_2, t)), \\
 \frac{\Delta J_5(\mathbf{x}, t)}{\Delta \mathbf{x}_5} &= J_5(\mathbf{x}, t) - J_5(\mathbf{x} - \mathbf{s}_5, t) = r_5 \frac{x_1(x_1 - 1)x_2}{2} p(x_1, x_2, t) \\
 &\quad - r_5 \frac{(x_1 - 1)(x_1 - 2)x_2}{2} p(x_1 - 1, x_2 + 1, t)/2, \\
 \frac{\Delta J_6(\mathbf{x}, t)}{\Delta \mathbf{x}_6} &= -(J_6(\mathbf{x}, t) - J_6(\mathbf{x} + \mathbf{s}_6, t)) = -\left(r_6 \frac{(x_1 - 1)x_1(x_1 + 1)}{6} p(x_1 + 1, x_2 - 1, t) \right. \\
 &\quad \left. - r_6 \frac{x_1(x_1 - 1)(x_1 - 2)}{6} p(x_1, x_2, t)\right).
 \end{aligned}$$

Total Reactional Flux and Velocity, Discrete Divergence, and Continuity Equation. Following Eq. (10), the total reactional flux $\mathbf{J}_r(\mathbf{x}, t) \in \mathbb{R}^6$ is:

$$\mathbf{J}_r(\mathbf{x}, t) = (J_1(\mathbf{x}, t), J_2(\mathbf{x}, t), J_3(\mathbf{x}, t), J_4(\mathbf{x}, t), J_5(\mathbf{x}, t), J_6(\mathbf{x}, t)),$$

where $\{J_k(\mathbf{x}, t)\}$ are as specified in Eq. (25). The total reactional velocity $\mathbf{v}_r(\mathbf{x}, t) \in \mathbb{R}^6$ is: $\mathbf{v}_r(\mathbf{x}, t) = \mathbf{J}_r(\mathbf{x}, t)/p(\mathbf{x}, t)$.

The discrete divergence $\nabla_d \cdot \mathbf{J}_r(\mathbf{x}, t)$ of the r-flux $\mathbf{J}_r(\mathbf{x}, t) \in \mathbb{R}^6$ over the discrete increments \mathbf{s}_k can be written as:

$$\nabla_d \cdot \mathbf{J}_r(\mathbf{x}, t) = \sum_{k=1}^6 \frac{\Delta J_k(\mathbf{x}, t)}{\Delta \mathbf{x}_k}. \quad (26)$$

The r-flux $\mathbf{J}_r(\mathbf{x}, t)$ indeed satisfies the continuity equation, as we have $\nabla_d \cdot \mathbf{J}_r(\mathbf{x}, t) = -\partial p(\mathbf{x}, t)/\partial t$ from Eqs. (13), (24), and (26)

Stoichiometry projection and single-reactional species flux. The single-reactional flux $J_k(\mathbf{x}, t)$ along the direction of reaction R_k can be decomposed into components of individual species using the predetermined stoichiometry $\mathbf{s}_k = (s_k^1, s_k^2)$. The x_1 and x_2 components of *stoichiometric projections* of $J_k(\mathbf{x}, t)$ are listed in Table 2. The single-reactional species flux is formed as follows:

$$\mathbf{J}_k(\mathbf{x}, t) \equiv (J_k^1(\mathbf{x}, t), J_k^2(\mathbf{x}, t)), \quad k = 1, \dots, 6, \quad (27)$$

where $J_k^1(\mathbf{x}, t)$ and $J_k^2(\mathbf{x}, t)$ listed in Table 2. The single-reactional species velocity $\mathbf{v}_k(\mathbf{x}, t) \in \mathbb{R}^2$ is $\mathbf{v}_k(\mathbf{x}, t) \equiv \mathbf{J}_k(\mathbf{x}, t)/p(\mathbf{x}, t)$.

Total Species Flux and Velocity. Following Eqs. (14)–(15), the total flux $\mathbf{J}_s(\mathbf{x}, t) \in \mathbb{R}^2$ is $\mathbf{J}_s(\mathbf{x}, t) = \sum_{k=1}^m \mathbf{J}_k(\mathbf{x}, t)$, where $\{\mathbf{J}_k\}$ as specified in Eq. (27). The total species velocity $\mathbf{v}_s(\mathbf{x}, t) \in \mathbb{R}^2$ is: $\mathbf{v}_s(\mathbf{x}, t) = \mathbf{J}_s(\mathbf{x}, t)/p(\mathbf{x}, t)$.

Overall Behavior of Schnakenberg System. We examine the behavior of the Schnakenberg system with $(a, b) = (10, 50)$ under two initial conditions, namely, that of the uniform distribution and $p(\mathbf{x} = (0, 0))|_{t=0} = 1$. We computed the time-evolving probability landscape $p = p(\mathbf{x}, t)$ using the ACME method [12, 43].

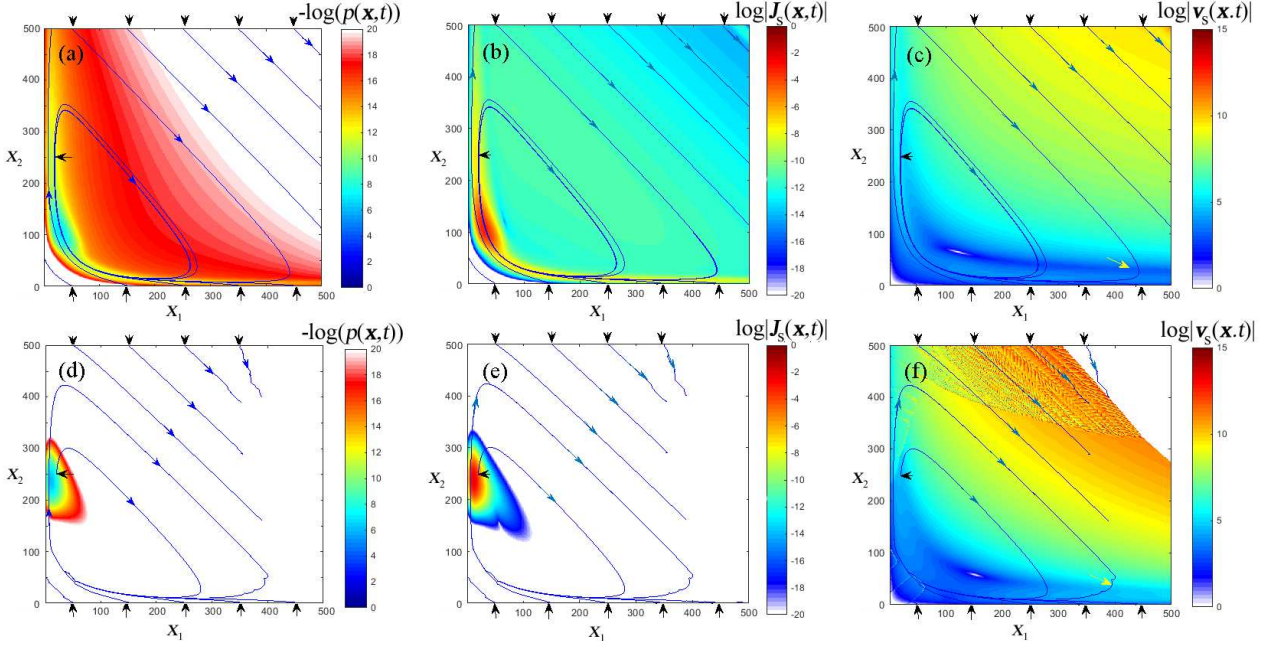


Figure 4: The time-evolving probability landscape, flux, and velocity of probability mass in the Schnakenberg system with $(a, b) = (10, 50)$ at $t = 0.5$, starting from the uniform distribution (a–c) and from the initial conditions of $p(\mathbf{x} = (0, 0))|_{t=0} = 1$ (d–f). a) and d): the probability landscape in $-\log(p(\mathbf{x}, t))$; b) and e): the corresponding value of flux in $\log |\mathbf{J}_s(\mathbf{x}, t)|$; c) and f): the log absolute value of velocity $\log |\mathbf{v}_s(\mathbf{x}, t)|$.

For the uniform distribution, the probability landscape in $-\log p(\mathbf{x}, t)$ at time $t = 0.5$ is shown in Figure 4a, where high probability regions are in blue. Its overall shape takes the form of closed valley, which is similar to an earlier study based on a Fokker-Planck model [18]. The trajectories of the flux field $\mathbf{J}_s(\mathbf{x}, t)$ at time $t = 0.5$ in the space of the copy-numbers from different starting locations (marked by black arrows at top and bottom) are shown in blue on Fig. 4–5. These trajectories depict the directions of the movement of the probability mass at different locations after traveling from the starting points. The heatmaps of the flux in $\log |\mathbf{J}_s(\mathbf{x}, t)|$ and the velocity in $\log |\mathbf{v}_s(\mathbf{x}, t)|$ are shown in Fig. 4b and Fig. 4c, respectively. The flux lines are closed curves and are overall smooth. These closed flux lines reflect the oscillatory nature of the reaction system. The velocity has larger values at locations where the flux trajectories are straight lines (green and yellow region in the upper right corner, Figure 4c), but drops significantly when the trajectories make down-right turns (light and dark blue in the lower right corner, marked with a yellow arrow).

For the initial conditions of $p(\mathbf{x} = (0, 0))|_{t=0} = 1$, $-\log p(\mathbf{x}, t)$ at time $t = 0.5$ is shown in Figure 4d, where high probability regions (blue) is located at a small neighborhood around $\mathbf{x} = (0, 250)$. The heatmaps of the flux in $\log |\mathbf{J}_s(\mathbf{x}, t)|$ and the velocity in $\log |\mathbf{v}_s(\mathbf{x}, t)|$ are shown in Fig. 4e and Fig. 4f, respectively. The flux lines are closed curves and are overall smooth. The oscillating flux lines appear again (Figs 4d–4f), but not all form closed curves. Specifically, all flux lines which start at the upper region ($x_2 = 500$)

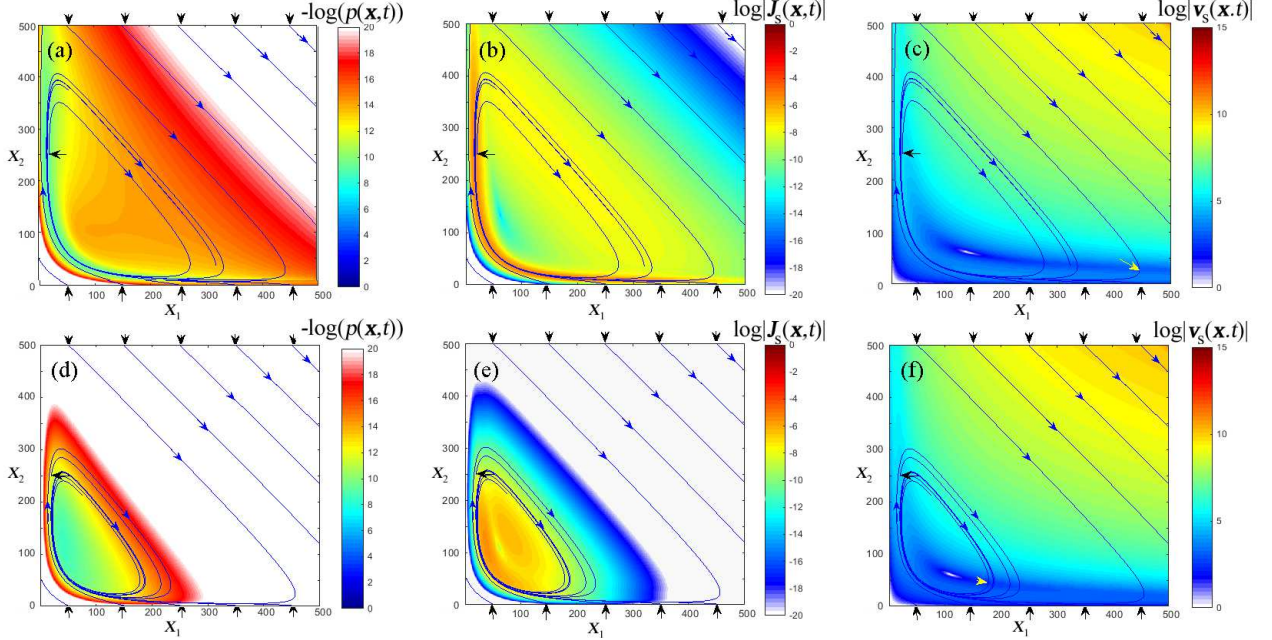


Figure 5: The steady-state probability landscape, flux, and velocity of probability mass in the Schnakenberg system with $(a, b) = (10, 50)$ (a–c) and $(a, b) = (20, 40)$ (d–f). a) and d): the probability landscape in $-\log(p(\mathbf{x}, t))$; b) and e): the corresponding values of flux in $\log|\mathbf{J}_s(\mathbf{x}, t)|$; c) and f): the log absolute value of velocity $\log|\mathbf{v}_s(\mathbf{x}, t)|$.

become broken-off in the mid-region, where the probability mass becomes negligible, resulting in negligible flux as well, with its absolute value close to be zero. The maximum of the flux is reached at the peak of the probability landscape (Figure 4e). The heatmap of the probability velocity exhibits a similar pattern as that of uniform distribution (Figure 4f vs. Figure 4c). The color palettes encoding the values of the velocity $\log|v_s(\mathbf{x}, t)|$ are not-smooth (Figure 4f). This is likely due to small numerical values of probability in this region.

We then examined the steady state behavior of the system at two conditions of the copy numbers of species A and B : $(a, b) = (10, 50)$ and $(a, b) = (20, 40)$. The probability landscape in $-\log(p(\mathbf{x}, t))$ for $(a, b) = (10, 50)$ shown in Fig. 5a exhibits similar shape to that of Fig. 4. The probability values are higher in locations near the left ($x_1 = 0$) and lower ($x_2 = 0$) boundaries. The flux lines (Fig. 5a–5c) move from the upper left corner to the lower right corner, and then make sharp right turns until reaching the neighborhood near the origin. Subsequently, they make right turns again and move upward, until the cycles are closed. These closed flux curves move along the contours on the probability landscape. The absolute values of the flux (Fig. 5b) are largest near the boundaries of the probability surfaces ($x_1 = 0$ and $x_2 = 0$, red/orange colored ridge) and nextly along the flux lines on the diagonal. The flux has small values in the region above the diagonal (cyan and blue). The heatmap of the velocity (Fig. 5c) exhibit a different pattern, with its value dropping significantly in the small blue arch (see region pointed by the yellow arrow), where flux lines make turns in the lower region.

The probability landscape in $-\log(p(\mathbf{x}, t))$ for $(a, b) = (20, 40)$ is shown in Fig. 5d. While exhibiting overall similar pattern to that of $(a, b) = (10, 50)$, the high probability regions is more concentrated in locations near the lower-left (Fig. 5d). The flux lines (Fig. 5d–f) are similar to those of $(a, b) = (10, 50)$ corner, but oscillate around much smaller contour, where $x_1 \leq 200$ and $x_2 \leq 300$. The close cycles of flux lines also move along the contours on the probability landscape.

The results obtained here are generally consistent with that obtained using a Fokker-Planck flux model computed from a landscape constructed using Gillespie simulations [8, 18]. For example, the directions of the

flux lines are the same. However, there are some differences. While the flux lines from the Fokker-Planck model exhibit oscillating behavior even in the boundary regions where $x_1 < 2$ or $x_2 < 2$, where reactions R_5 and R_6 cannot occur hence no oscillating flux are physically possible. No such inconsistency exist in our model. Furthermore, the system considered here is much larger, with hundreds of copies of X_1 and X_2 involed, whereas < 10 copies of X_1 and X_2 were considered in [18].

4 Conclusion

In this study, we introduce new formulations of discrete flux and discrete velocity for an arbitrary mesoscopic reaction system. Specifically, we redefine the derivative and divergence operators based on the discrete nature of chemical reactions. We then introduce the discrete form of continuity equation for the systems of reactions. We define two types of discrete flux, with their relationship specified. The reactional discrete flux satisfies the continuity equation and describes the behavior of the system evolving along directions of reactions. The species flux directly describes the dynamic behavior of the reactions such as the transfer of probability mass in the state space. Our discrete flux model enables the construction of the global time-evolving and steady-state flow-maps of fluxes in all directions at every microstate. Furthermore, it can be used to tag the fluxes of outflow and inflow of probability mass as reactions proceeds. In addition, we can now impose boundary conditions, allowing exact quantification of vector fields of the discrete flux and discrete velocity anywhere in the discrete state space, without the difficulty of enforcing artificial reflecting conditions at the boundaries [42]. We note that the accurate construction of the discrete probability flux, velocity, and their global flow-maps requires the accurate calculation of the time-evolving probability landscape of the reaction network. This is made possible by using the recently developed ACME method [12, 43].

As a demonstration, we computed the time-evolving probability flux and velocity fields for three model systems, namely, the birth-death process, the bistable Schlögl model, and the oscillating Schnakenberg system. We showed how flux and velocities converge to zero when the system reaches the steady-state in the birth-death process and the Schlögl models. We also showed that the flux and velocity trajectories in the Schnakenberg system converge to the oscillating contours of the steady-state probability landscape, similar to an earlier study [18], although there are important differences. Overall, the general framework of discrete flux and velocity and the methods introduced here can be applied to other networks and dynamical processes involving stochastic reactions. These applications can be useful in quantification of dynamic changes of probability mass, identification as well as characterization of mechanism where movement of probability mass drives the system towards the steady-state. They may also aid in our understanding of the mechanisms that determined the non-equilibrium steady state of many reaction systems.

5 Acknowledgments

Support from NIH R35 GM127084 and NSF DMS-1714401 is gratefully acknowledged.

References

- [1] Harley H McAdams and Adam Arkin. It's a noisy business! genetic regulation at the nanomolar scale. *Trends in Genetics*, 15(2):65–69, 1999.
- [2] Harley H McAdams and Adam Arkin. Stochastic mechanisms in gene expression. *Proceedings of the National Academy of Sciences*, 94(3):814–819, 1997.
- [3] Mads Kærn, Timothy C Elston, William J Blake, and James J Collins. Stochasticity in gene expression: from theories to phenotypes. *Nature Reviews Genetics*, 6(6):451–464, 2005.
- [4] Vahid Shahrezaei, Julien F Ollivier, and Peter S Swain. Colored extrinsic fluctuations and stochastic gene expression. *Molecular Systems Biology*, 4(1):196, 2008.

- [5] Michael B Elowitz, Arnold J Levine, Eric D Siggia, and Peter S Swain. Stochastic gene expression in a single cell. *Science*, 297(5584):1183–1186, 2002.
- [6] Peter S Swain, Michael B Elowitz, and Eric D Siggia. Intrinsic and extrinsic contributions to stochasticity in gene expression. *Proceedings of the National Academy of Sciences*, 99(20):12795–12800, 2002.
- [7] Melissa Vellela and Hong Qian. A quasistationary analysis of a stochastic chemical reaction: Keizer’s paradox. *Bulletin of Mathematical Biology*, 69(5):1727–1746, 2007.
- [8] Daniel T Gillespie. Exact stochastic simulation of coupled chemical reactions. *The Journal of Physical Chemistry*, 81(25):2340–2361, 1977.
- [9] Huy D Vo and Roger B Sidje. An adaptive solution to the chemical master equation using tensors. *The Journal of chemical physics*, 147(4):044102, 2017.
- [10] Verena Wolf, Rushil Goel, Maria Mateescu, and Thomas A Henzinger. Solving the chemical master equation using sliding windows. *BMC Systems Biology*, 4(1):42, 2010.
- [11] Kevin Burrage, MARKUS Hegland, Shev Macnamara, Roger Sidje, et al. A krylov-based finite state projection algorithm for solving the chemical master equation arising in the discrete modelling of biological systems. In *Proc. of The AA Markov 150th Anniversary Meeting*, number 21-37, 2006.
- [12] Youfang Cao, Anna Terebus, and Jie Liang. State space truncation with quantified errors for accurate solutions to discrete chemical master equation. *Bulletin of Mathematical Biology*, 78(4):617–661, 2016.
- [13] Youfang Cao and Jie Liang. Adaptively biased sequential importance sampling for rare events in reaction networks with comparison to exact solutions from finite buffer dcme method. *The Journal of Chemical Physics*, 139(2):07B605_1, 2013.
- [14] RKP Zia and B Schmittmann. Probability currents as principal characteristics in the statistical mechanics of non-equilibrium steady states. *Journal of Statistical Mechanics: Theory and Experiment*, 2007(07):P07012, 2007.
- [15] Chunhe Li, Erkang Wang, and Jin Wang. Landscape, flux, correlation, resonance, coherence, stability, and key network wirings of stochastic circadian oscillation. *Biophysical Journal*, 101(6):1335–1344, 2011.
- [16] Xue-Juan Zhang, Hong Qian, and Min Qian. Stochastic theory of nonequilibrium steady states and its applications. part i. *Physics Reports*, 510(1):1–86, 2012.
- [17] Jin Wang, Li Xu, and Erkang Wang. Potential landscape and flux framework of nonequilibrium networks: robustness, dissipation, and coherence of biochemical oscillations. *Proceedings of the National Academy of Sciences*, 105(34):12271–12276, 2008.
- [18] Liufang Xu, Hualin Shi, Haidong Feng, and Jin Wang. The energy pump and the origin of the non-equilibrium flux of the dynamical systems and the networks. *The Journal of Chemical Physics*, 136(16):165102, 2012.
- [19] Ruoshi Yuan, Xinan Wang, Yian Ma, Bo Yuan, and Ping Ao. Exploring a noisy van der pol type oscillator with a stochastic approach. *Physical Review E*, 87(6):062109, 2013.
- [20] Michael Strasser, Fabian J Theis, and Carsten Marr. Stability and multiattractor dynamics of a toggle switch based on a two-stage model of stochastic gene expression. *Biophysical Journal*, 102(1):19–29, 2012.
- [21] J Tse Margaret, Brian K Chu, Mahua Roy, and Elizabeth L Read. Dna-binding kinetics determines the mechanism of noise-induced switching in gene networks. *Biophysical Journal*, 109(8):1746–1757, 2015.

- [22] Luciana Renata de Oliveira, Armando Bazzani, Enrico Giampieri, and Gastone C Castellani. The role of non-equilibrium fluxes in the relaxation processes of the linear chemical master equation. *The Journal of Chemical Physics*, 141(6):08B608_1, 2014.
- [23] C Bianca and A Lemarchand. Evaluation of reaction fluxes in stationary and oscillating far-from-equilibrium biological systems. *Physica A: Statistical Mechanics and its Applications*, 438:1–16, 2015.
- [24] Chunhe Li and Jin Wang. Landscape and flux reveal a new global view and physical quantification of mammalian cell cycle. *Proceedings of the National Academy of Sciences*, 111(39):14130–14135, 2014.
- [25] Jin Wang, Li Xu, Erkang Wang, and Sui Huang. The potential landscape of genetic circuits imposes the arrow of time in stem cell differentiation. *Biophysical Journal*, 99(1):29–39, 2010.
- [26] Chunhe Li and Jin Wang. Quantifying the underlying landscape and paths of cancer. *Journal of The Royal Society Interface*, 11(100):20140774, 2014.
- [27] Ying Tang, Ruoshi Yuan, Gaowei Wang, Xiaomei Zhu, and Ping Ao. Potential landscape of high dimensional nonlinear stochastic dynamics with large noise. *Scientific Reports*, 7:15762, 2017.
- [28] Paul Sjöberg, Per Lötstedt, and Johan Elf. Fokker–planck approximation of the master equation in molecular biology. *Computing and Visualization in Science*, 12(1):37–50, 2009.
- [29] Chung Yuan Mou, Jiu-li Luo, and Gregoire Nicolis. Stochastic thermodynamics of nonequilibrium steady states in chemical reaction systems. *The Journal of Chemical Physics*, 84(12):7011–7017, 1986.
- [30] Tim Schmiedl and Udo Seifert. Stochastic thermodynamics of chemical reaction networks. *The Journal of Chemical Physics*, 126(4):044101, 2007.
- [31] Shixin Xu, Ping Sheng, and Chun Liu. An energetic variational approach for ion transport. *arXiv preprint arXiv:1408.4114*, 2014.
- [32] Daniel Schultz, Aleksandra M Walczak, José N Onuchic, and Peter G Wolynes. Extinction and resurrection in gene networks. *Proceedings of the National Academy of Sciences*, 105(49):19165–19170, 2008.
- [33] Ying Tang, Ruoshi Yuan, and Ping Ao. Nonequilibrium work relation beyond the boltzmann-gibbs distribution. *Physical Review E*, 89(6):062112, 2014.
- [34] Nicolaas Godfried Van Kampen. *Stochastic processes in physics and chemistry*. Elsevier, 2007.
- [35] Ramon Grima, Philipp Thomas, and Arthur V Straube. How accurate are the nonlinear chemical fokker-planck and chemical langevin equations? *The Journal of Chemical Physics*, 135(8):084103, 2011.
- [36] Andrew Duncan, Shuohao Liao, Tomáš Vejchodský, Radek Erban, and Ramon Grima. Noise-induced multistability in chemical systems: Discrete versus continuum modeling. *Physical Review E*, 91(4):042111, 2015.
- [37] Daniel T Gillespie. The chemical langevin equation. *The Journal of Chemical Physics*, 113(1):297–306, 2000.
- [38] Florence Baras, M Malek Mansour, and JE Pearson. Microscopic simulation of chemical bistability in homogeneous systems. *The Journal of Chemical Physics*, 105(18):8257–8261, 1996.
- [39] Peijie Zhou and Tiejun Li. Construction of the landscape for multi-stable systems: Potential landscape, quasi-potential, a-type integral and beyond. *The Journal of Chemical Physics*, 144(9):094109, 2016.
- [40] Armando Bazzani, Gastone C Castellani, Enrico Giampieri, Daniel Remondini, and Leon N Cooper. Bistability in the chemical master equation for dual phosphorylation cycles. *The Journal of Chemical Physics*, 136(23):06B611, 2012.

- [41] Jordan M Horowitz and Massimiliano Esposito. Thermodynamics with continuous information flow. *Physical Review X*, 4(3):031015, 2014.
- [42] Alessandro Ceccato and Diego Frezzato. Remarks on the chemical fokker-planck and langevin equations: Nonphysical currents at equilibrium. *The Journal of Chemical Physics*, 148(6):064114, 2018.
- [43] Youfang Cao, Anna Terebus, and Jie Liang. Accurate chemical master equation solution using multi-finite buffers. *Multiscale Modeling & Simulation*, 14(2):923–963, 2016.
- [44] Bernie J Daigle Jr, Min K Roh, Dan T Gillespie, and Linda R Petzold. Automated estimation of rare event probabilities in biochemical systems. *The Journal of Chemical Physics*, 134(4):01B628, 2011.
- [45] Linda JS Allen. *An introduction to stochastic processes with applications to biology*. CRC Press, 2010.
- [46] Friedrich Schlögl. Chemical reaction models for non-equilibrium phase transitions. *Zeitschrift für Physik*, 253(2):147–161, 1972.
- [47] Hong Qian, Saveez Saffarian, and Elliot L Elson. Concentration fluctuations in a mesoscopic oscillating chemical reaction system. *Proceedings of the National Academy of Sciences*, 99(16):10376–10381, 2002.
- [48] Youfang Cao and Jie Liang. Nonlinear langevin model with product stochasticity for biological networks: the case of the schnakenberg model. *Journal of Systems Science and Complexity*, 23(5):896–905, 2010.
- [49] Donald A McQuarrie. Stochastic approach to chemical kinetics. *Journal of Applied Probability*, 4(3):413–478, 1967.
- [50] Youfang Cao and Jie Liang. Optimal enumeration of state space of finitely buffered stochastic molecular networks and exact computation of steady state landscape probability. *BMC Systems Biology*, 2(1):30, 2008.
- [51] Youfang Cao, Hsiao-Mei Lu, and Jie Liang. Probability landscape of heritable and robust epigenetic state of lysogeny in phage lambda. *Proceedings of the National Academy of Sciences*, 107(43):18445–18450, 2010.
- [52] Ramamurti Shankar. *Principles of quantum mechanics*. Springer Science & Business Media, 2012.
- [53] Hao Ge, Min Qian, and Hong Qian. Stochastic theory of nonequilibrium steady states. part ii: Applications in chemical biophysics. *Physics Reports*, 510(3):87–118, 2012.
- [54] Melissa Vellela and Hong Qian. Stochastic dynamics and non-equilibrium thermodynamics of a bistable chemical system: the schlögl model revisited. *Journal of The Royal Society Interface*, 6(39):925–940, 2009.
- [55] J Schnakenberg. Network theory of microscopic and macroscopic behavior of master equation systems. *Reviews of Modern Physics*, 48(4):571, 1976.